QUANTITATIVE ASSESSMENT OF AUTOMATED CRATER DETECTION ON MARS

Jung Rack **Kim** [a], Jan-Peter Muller, Jeremy G **Morley**

Dept. of Geomatic Engineering, University College London, Gower Street, London, WC1E 6BT UK
jkim@ge.ucl.ac.uk [a]

WG VI/9

KEY WORDS: Extra-terrestrial, DEM/DTM, Feature, Geomorphology, Vision, Automated crater detection

ABSTRACT:

Crater Size-Frequency Distributions (SFD) on planetary surfaces are crucial to dating the geological age. On the Moon they have been employed together with radioactive K-Ar techniques to determine ages of different regions. The launch of the ESA Mars Express (MEX) mission on 6 June 2003 with the 9-view camera HRSC (High Resolution Stereo Camera) orbiting instrument and subsequent spectacular multi-angle and colour data acquired since January 2004 opens up the possibility of applying the lessons learnt on the Moon to Mars. Although there is an on-line web-based cataloguing and mapping system at USGS which shows the location and characteristics of some 40,000 craters on Mars (Mars Crater Consortium, MCC) with diameters >5km, these craters represent only a tiny fraction of the millions of craters which are believed to be present on the Martian surface. It is highly unlikely that there will ever be sufficient resources to map these smaller craters using existing manually-intensive techniques. An automated crater detection algorithm has been developed which exploits both image data and DTMs derived from laser altimetry (MGS-MOC) and in future DTMs from HRSC. The algorithm is described and examples of it's application for a variety of different crater types are demonstrated. Central to the application of any automated algorithm and prior to systematic application to the Martian planetary surface it is crucial to perform a quantitative assessment of any automated algorithm's performance. We show results from three different approaches here: (1) inter-comparison of automated crater locations with those in the MCC catalogue; ; (2) inter-comparison of automated crater locations with manually-derived crater locations; (3) simulation of crater images using an idealised 3D model of a Martian crater changing the illumination conditions.

1. INTRODUCTION

1.1 Aims

Impact crater detection and crater size frequency counting have a very high priority in Extra Terrestrial Mapping and planetary chronological research. In spite of the increasing demand for geological and geodetic control over the last few decades, the application of machine vision to address this problem has not been very successful. The main reasons can be summarized as follows:.

a) The "visibility" of impact craters in optical images depends not only on the surface scattering behaviour but also on the illumination direction, atmospheric state as well as the sensor incidence direction.
b) Some geographical features like small valleys and volcanoes have similar morphological characteristics as craters in low-level feature space.
c) Impact craters are often concentrated into clusters resulting in overlap and for larger structures, multi-ring structures frequently occur. This means that the separation of individual craters from their background can be very difficult to generalise.
d) Craters on Mars are frequently eroded due to surface (aeolian processes such as dust storms as well as the action of water.

To address these problems, a combinatorial fusion technique has been developed to exploit not only image features bur crucially 3D information. The final objective is to develop a fully automated processing system which can accurately detect boundary rims of impact craters using raw planetary images and 3D data with sufficient accuracy for practical planetary research. Here we report on an evaluation of the crater detected products with simulated crater features, manually detected craters and the MCC (Mars Crater Consortium) catalogue (Barlow, 2003).

1.2 Previous research work

Several methods to automatically detect craters have been developed but are not operational yet. The first data mining system for planetary images including the functionality for impact crater detection was Diamond Eye (Burl et al. 1999). No quantitative evaluation was reported. Another case of impact crater detection on an asteroid, which appears to be relatively successful is Leroy et al. (2001)'s work. The primary aim of this research was the automated detection of impact crater and 3D modelling of asteroids. Recently, Michael (2002) developed a crater detection algorithm using an elliptical Hough transformation applied to a global MOLA DTM. His result was apparently very successful so that the correct shift vector between the MDIM and MOLA DEM could be extracted using this information. Magee et al. (2003) showed an automated impact carter detection by edge processing and template matching. Kim and Muller (2003) suggested a similar crater detection method but employing ellipse fitting on the DTM and optical image.

2. ALGORITHMS

The overall processing steps are shown in Figure 1. The procedure consists of 3 stages. Firstly, target edge segments in so-called ROIs (Region of Interests) are defined in a focusing stage using a GLCM (Grey Level Co-occurrence Matrix) texture classifier and edge direction analysis. These "Preliminary crater edges" are then organized to find optimal ellipses in a second processing step. Optimal ellipses for impact craters are evaluated using a fitness function and refined using a

Hough transformation. They are then finally verified using template matching.
In the case of small impact craters, which are classified by measuring their ROIs' size, the RoIs are directly fitted to an optimal ellipse without any further processing.

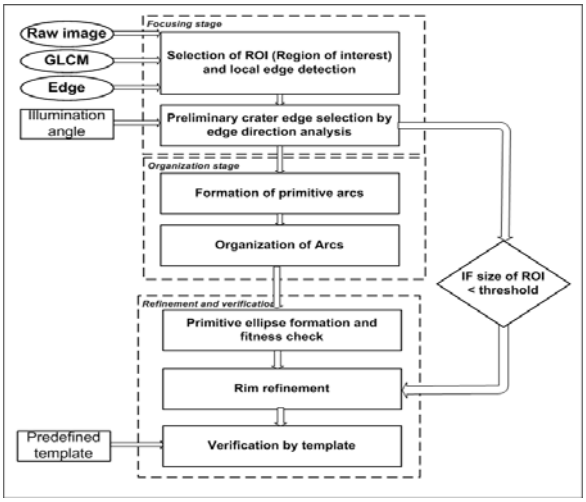

Figure 1. Overall work flow and processing steps

2.1 Focusing

When applying the first stage, there are usuallye too many connected edge segments in an optical image. For example, hundreds of edges appear in a single MOC image even on a relatively flat area. Therefore it is impossible to apply these algorithms to these edges to drive crater shape. A focusing strategy using the GLCM and edge direction analysis is used here to reduce the search space.
At first, an edge is localized by it's ROI, which is defined through GLCM texture classification. Then within a localized edge area, edge thresholding is applied.
However, extracted edges usually include not only crater rims but also shadow boundaries. As seen in Figure 3, which is generated from a generalised 3D crater using a Phong shading model, four different shading regions can be defined and the boundaries of each shading form double structured edge lines. The real crater edge is usually the boundary between the illuminated and shadowed areas.

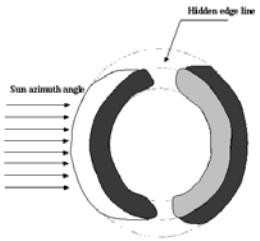

Figure 2. Edge formation geometry in specific illumination condition

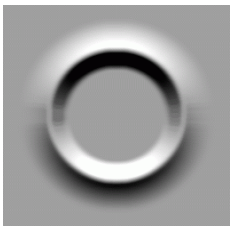

(a) Simulated image using hill shading for a crater DTM model using a Phong shading model Solar Evevation =45°, Solar Azimuth=0°)

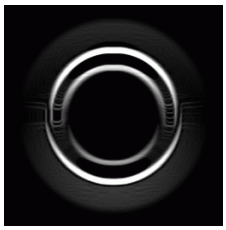

(b) Detected edges from image (a)

Figure 3. Simulated crater image and edges

The analysis of edges in these four regions by looking at the directional properties shows that the centre point of the crater rim part should satisfy the following condition.

$$\theta + \varphi = \frac{\pi}{2} \qquad (1)$$

where θ = sun azimuth angle,
φ=edge direction of centre point

Additionally the extent of one crater edge rim is limited by

$$\varphi_c - \pi/2 < \varphi < \varphi_c + \pi/2 \qquad (2)$$

where φ_c = edge direction of centre point ,
φ =edge direction of crater rim

assuming that there are no hidden edge lines from erosion or other illumination effects.
The detection of preliminary crater edge can be simply implemented by rotating the edge mask or a algorithms discussed below.
At first, the marginal degree of the central peak is defined in individual ROIs by (3),

$$\varphi_m = \frac{2\pi}{0.5\max(Dx, Dy)} \qquad (3)$$

where Dx = X dimension,
Dy =Y dimension of connected component

so that if the thresholded part includes edge segment, which satisfy (4)

$$\varphi_c + \varphi_m < \varphi < \varphi_c + \varphi_m \quad (4)$$

where φ_c: edge direction of centre point.
Then we can define this as a preliminary crater rim edge. Then re-arranging all of the edge pixels with r (estimated centre from initial conic fitting) and φ space after finding the maximum intensity point in each φ_s interval to detect seed points. By applying region growing with these seed points using

4 connectivity within a fixed edge intensity level, the extent of preliminary crater rim edges can be precisely defined as seen in Figure 4.

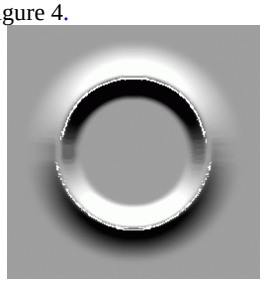

(a) Rim edge detection from simulated image

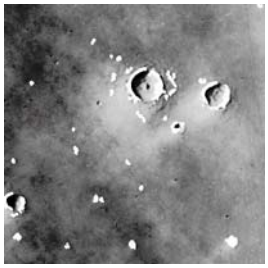

(b) Rims detected in MOC optical image image (MOC WA image M0103863)

Figure 4. Preliminary crater rim detection results

2.2 Edge Organization

The preliminary crater rims are defined in the focusing stage. However, it is necessary to organize these edges into more useful and general shapes, particularly an optimal ellipse (in the case of a geometrically corrected image, it is usually a circle). The most well known edge organization method for circle or ellipse detection is the Hough transformation and there are a lot of modified versions for efficient detection of ellipses or circles (Atherton and Kerbyson, 1999, Yuen at al. 1989, Olson 1998). However, none of them appear to be sufficiently robust to guarantee the reliable detection of impact craters from the preliminary crater rim edge according to our experience. Here, we address this problem using conic section fitting.

Among several conic section fitting methods, two algorithms are employed in our scheme. One is Pilu's Direct Least Squared (DLS) fitting method (Pilu et al, 1999) and the other is Kanazawa and Kanantani (1996)'s conic fitting by optimal estimation (OE). Both appear to be reliable even with quite noisy data but Kanazawa and Kanantani's fitting scheme shows much higher accuracy with relatively short arcs, which are frequently observed in Martian crater rims. Kanantani and Ohta (2004) developed an osculating ellipse (OE) detection algorithm by fitting conic sections but their method only appears to work if the edge segment covers more than half of the ellipse. This assumption is usually not valid for most of the impact craters (>100 pixels in optical image), where one connected edge frequently covers only a small percentage of an ellipse according to our experience. On the other hand, the CPU cost of Kanazawa and Kanantani's covariance tensor approach and iterative renormalization is quite expensive compared with Pilu's DLS fitting scheme. Therefore, we developed an edge organization scheme, which employs DLS fitting for an intermediate stage and refines organized edges by OE fitting. It consists of two sub-stages: primitive arc definition and arc organization.

At first the possible path map is constructed using the following condition.

$$Max\ (S_{ix}, S_{iy}) + Max\ (S_{jx}, S_{jy}) < \|C_i - C_j\| \qquad (5)$$

where S_{ix}, S_{jx} : geometrical x size of edge segment i,j,
Ci,Cj : centre location of edge segment I,j

Then a check is made of fitness for every possible arc pairs by (6), which measures the matching ratio between the fitted conic and edge points.

$$Fitness = \sum_{(i,j)\in E} T(i,j) / \sum_{(i,j)} E(i,j) \qquad (6)$$
$$E = e \oplus s$$

where T(i,j) : thresholded edge image
e(i,j) : binary image of fitted conic
s : kernel for binary erosion in size
n : 0.1*radius of fitted conic, if 0.1*radius < 1, n=1

If the score of such a fitness function is higher than a given threshold value, this is considered a primitive arc. These primitive arcs are then organised as optimal ellipses by other kinds of path checking procedure. If the overlap ratio between two primitive arcs is more than some pre-specified thresholding value, that path is considered as a possible one for optimal ellipse formation. The method for ellipse formation is a very simple process using the cycle detection in an undirected graph, which is constructed from the previous path search step.

(a) edge and fitted arc

(b) optimal preliminary ellipse

Figure 5. Ellipse organization

2.3 Refinement and verification

Onto the edge points of the optimal preliminary ellipses, OE conic fitting is applied and fitness is evaluated once more. If fitness is higher than a threshold value (usually 0.4), it is considered as a potential crater boundary. As seen in Figure 6 (a), the outlines of crater rims are not correctly matched with the finally fitted ellipse so that one more refinement step is necessary. This step uses a Hough transformation at several fixed radii and centre point ranges with different margins.

The final procedure for crater detection is the verification stage by template matching. As we already know the size of the detected crater, it is possible to examine the correlation value

between a predefined template and a detected crater ellipse. At first, the detected ellipse is resampled to a comparable size as the template and transformed to similar illumination conditions (sun azimuth angle is used here). Exact resizing and rotation is not feasible so that the Gruen (1991) image matching scheme, which has been the best solution for the registration between distorted image patches, is introduced to address geometrical distortions, due to effects such as foreshortening in the detected crater. The correlation value by caters of various sizes and shapes is illustrated in.

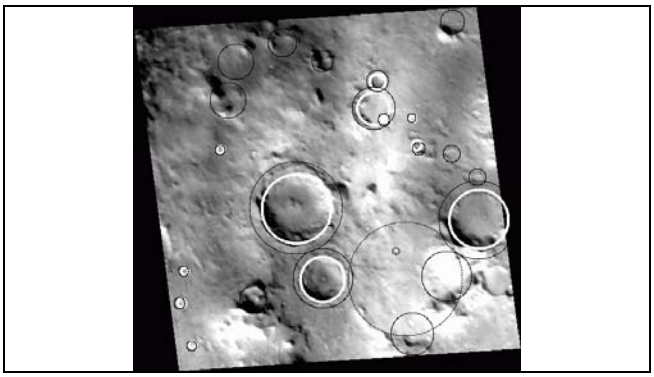

Figure 6. First outline of crater rim and refinement by Hough transformation and verification with template
(Black : verification range by hough and template matching, White : verified and refined crater MOC WA image M1103889)

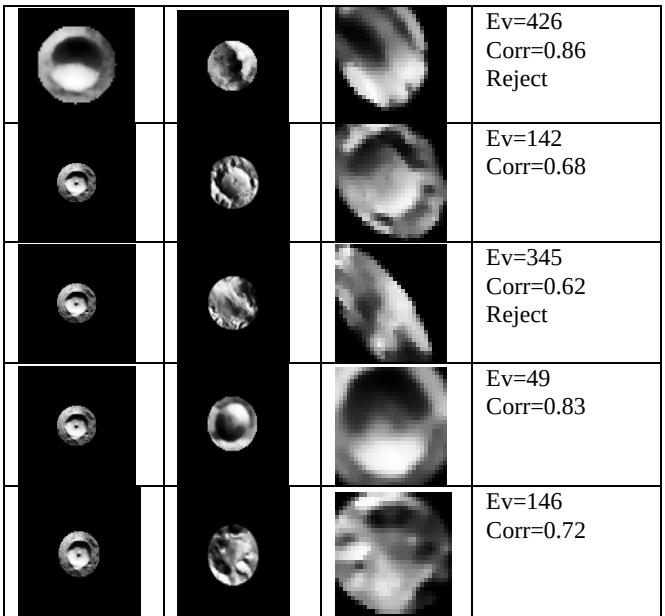

Figure 7. Correlation value by verification with template

2.4 Crater detection based on DTM

In some cases, the detection results on the optical image are poor, because the crater rim arcs are too short, which result from erosion, compared with their radii. To compensate for this, a DTM based crater detection is introduced.
It is much simpler than the corresponding optical image case. The focusing method is replaced with a high slope area extraction. Instead of using the local edge of the optical images, ridge points from a gridded DTM (Wood, 1996) are used for the ellipse fitting. The big impact craters, which are not detected in optical images due to insufficient robustness of the edge linking method, can be easily identified here.

3. RESULTS & ASSESSMENTS

Final products are evaluated by visual inspection and quantitative assessments are made through comparisons with MCC and manually detected crater ellipses.

3.1 Detection result on DEM

Crater detection is performed with a MOLA DTM, gridded at 256 m /pixel at the equator, which is shown in Figure 8. One characteristic of such DTM crater detection results is a high detection ratio for big craters with radii>15 km, even though the impact craters with small radii(< 4-5km) are usually not detected. Therefore it is highly complementary to the weakness of the detection results for optical images.

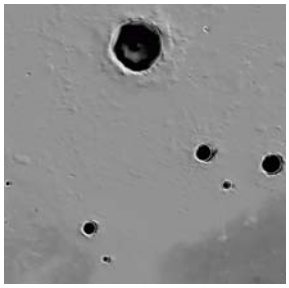

(a) E 99.226-101.58° N 23.375-25.72°

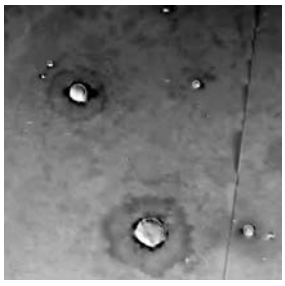

(b) E 119.476-121.828° N 20.828-23.164°

Figure 8. Crater detection on MOLA DTMs

3.2 Detection results on optical image

Several examples of crater detection evaluation are shown in Figure 9. The detection ratio of relatively small impact craters (8<R<about 60 pixel) is excellent but large or multi-ringed structured crater show relatively poor detection accuracy.
For quantitative assessment, quality assessment factors (Shufelt & McKeown, 1993), originally developed for building detection work, are introduced as follows:

$$\begin{aligned} &\text{Detection Percentage} = 100\,TP/(TP+FN) \\ &\text{Branching Factor} = FP/TP \\ &\text{Quality Percentage} = 100TP/(TP+FP+FN) \end{aligned} \quad (7)$$

where TP: TRUE POSITIVE - Both data sets (detected crater and comparison data set) classify the pixel as being part of a crater
TN: TRUE NEGATIVE - Both data sets classify the pixel as being part of the background
FP: FALSE POSITIVE - Detected data set classifies the pixel as a crater, comparison data set classifies it as background.
FN: FALSE NEGATIVE - Detected data set classifies the pixel as background, comparison data set classifies it as a crater

However, if we apply these factors directly to the optical image results, the detection ratio is likely to be very low, because the non-detection of large sized impact craters significantly reduces the detection ratio. So the QA factors are modified for impact craters, which have higher detection percentages than 50%, which are considered as true detection. Detection results by this scheme are shown in Table 1.

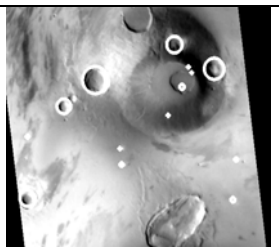

(a) Crater detection on MOC-WA level 2 image (M0203967)

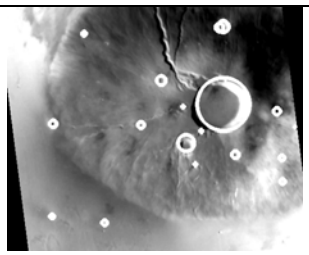

(b) Crater detection on MOC-WA level 2 image (M0203967)

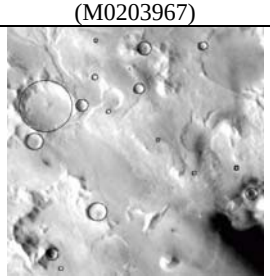

(e) Crater detection on MOC WA level 1 image M0300749

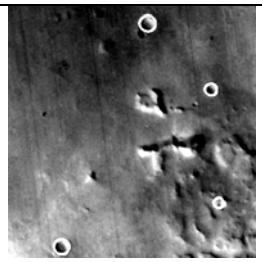

(f) Crater detection on MOC-WA level 2 image (M0900109)

Figure 9. Crater detection examples for craters of various sizes and shapes. Note that heavily eroded craters are not currently detected,

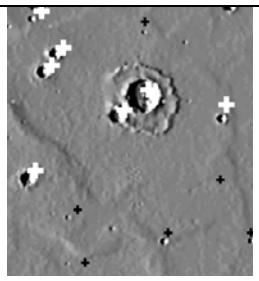

(a) Centre points of craters in MCC overlaid on MOLA DEM

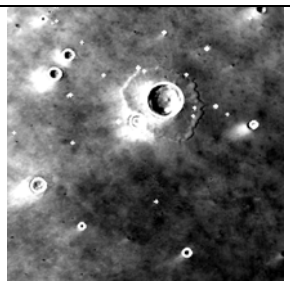

(b) Crater detection results with MOC-WA level 2 image (M0101958) same area with case (b)

Figure 10. Inter-comparison with MCC data sets and detected craters on MOC WA image (white + ; Barlow data sets , Black + : Kuzmin data sets)

	MCC (Barlow)	Manual measurement	
		Small size (R < 8 pixels)	Large Size (8 <R<60)
True positively detected crater number	60	198	120
False positively detected crater number	False positive has no meaning for the MCC inter comparison, because MCC data sets don't aim to catalogue all craters in target area	74	10
False negatively detected crater number	12	32	12
Detection percentage	83%	86%	90%
Branching factor	-	0.37	0.08
Quality percentage	-	65%	84%

*True negative has no meaning for individual crater detection

Table 1. Impact crater detection ratio by intercomparison with MCC and manual measurement in 12 random MOC WA images

3.3 Simulation with different illumination condition

As far as we have experienced, the illumination condition is crucial for the positional accuracy of the detected impact crater. To assess the robustness of an algorithm with different ranges of illumination angles, simulated crater DTMs whose diameter was 100 pixels and which have vertical 3D profiles of well known craters proposed by Duxbury (1991), was employed. Hill shaded images were generated at 10º intervals within the range of 0-360º sun azimuth angle and 20-90º elevation angles using a Minnaert surface's reflectance model which is given by (8).

$$P = B(\cos i'')^k (\cos e'')^{k-1} \qquad (8)$$

where B: brightness coefficient ,
k : the constant of Minnaert exponent
e: emission angle, I ; incidence angle

The results show very good agreement with actual (modelled) positions except at very high sun elevation angles around 90º, which rarely occurs for real image acquisitions.

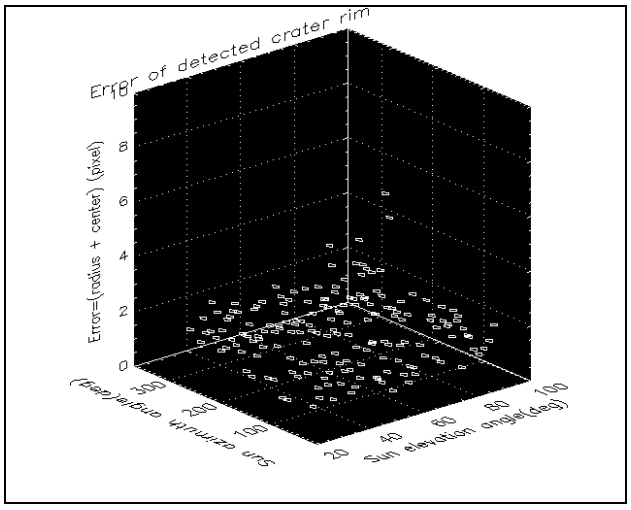

Figure 11. Detected impact crater's positioning accuracy in simulated data

4. CONCLUSION

Automated impact crater detection algorithms were developed to identify various sizes of impact craters under different conditions such as illumination angles and geographical complexity. The algorithm developed here shows a reliable detection accuracy for crater rim locations under many different conditions when the automated crater locations were compared against the MCC catalogue and manual measurements. Currently, the MCC catalogue covers craters, which have diameters >5km. The algorithm described here appears to have great potential for extending the range of the MCC catalogue to a much wider range of crater diameters especially with the release of new high resolution Mars optical images such as HRSC, where manual measurements are unlikely to be practicable.

REFERENCES

Atherton,T.J., Kerbyson,D.J.,1999, Size invariant circle detection, *Image and Vision computing*, 17(1), pp.795-803

Barlow, N. G., 2003. Revision of the “Catalog of large Martian impact craters” *International Conference on Mars*, 20-25 July, Pasadena, US. http://www.lpi.usra.edu/meetings/sixthmars2003/pdf/3073.pdf

Burl, M.C.,Fowlkes, C., Roden, J., Stechert, A., Mukhtar, S., 1999, Diamond Eye: A Distributed Architecture for Image Data Mining", *In SPIE Aerosense Conference: Data Mining and Knowledge Discovery, Orlando, US.*

Yuen, H.K., Illingworth, J., Kittler, J.V., 1989, Detecting Partially Occluded Ellipses Using the Hough Transform**,** *Image and vision computing*, 7(1), pp. 31-37.

Duxbury, T.C., 1991, An analytic model for the Phobos surface, *Planet Space Sci*., 39(1/2), pp. 355-376.

Gruen, A.W., 1985, Adaptive least squares correlation : a powerful image matching technique, *South African Journal of Photogrammetry Remote Sensing and Cartography*, 13(3), pp.175-187.

Kannatani, K., Ohta, N., 2004, Automatic detection of circular objects by ellipse growing, *International Journal of Image and Graphics*, 4(1), pp35-50.

Kanazawa, Y., Kannatani, K., 1996, Optimal conic fitting and reliability evalution, *Institute of Electronics, Information and Communication Engineering, Transaction on information and system*, E79-D(9), pp.1323-1328.

Kim,J. R., Muller, J-P., 2003, Impact crater detection on optical image and DEM, *ISPRS WG IV/9: Extraterrestrial Mapping Worksho,p"Advances in Planetary Mapping 2003", http://astrogeology.usgs.gov/Projects/ISPRS/MEETINGS/Houston2003/index_houston.html*

Leroy, B., Medioni, G.G., Johnson, E., Matthies, L., 2001, Crater detection for autonomous landing on asteroids. *Image and Vision Computing*, 19(11), pp.787-792.

Magee, M., Chapman, C.R., Dellenback, S.W., Enke, B., Merline,W.J., Rigney, M.P., 2003, Automated Identification of Martian craters using image processing**,** *Lunar and Planetary Science Conference* , Houston, US.,17-21 March.

Michael, G., 2002, Coordinate registration by automated crater detection, *Vernadsky/Brown Microsymposium on Comparitive Planetology***,** 27-29 October, Moscow Russia

Olson, C. F., 1999, Constrained Hough transformations for Curve detection, *Computer and Image Understanding* , 27(3),pp.329-345.

Pilu, M., Fitzgibbon, A., Fisher, R., 1999, Direct least square fitting of ellipses, *IEEE Transactions on Pattern Analysis and Machine Intelligence* 21 (5), pp.476-480.

Shufelt, J., McKeown, D.M., 1993. Fusion of monocular cues to detect man-made structures in aerial imagery, *Computer Vision and Image Understanding* 57(3) pp. 307-330.

Wood, J., 1996, The Geomorphological Characterisation of Digital Elevation Models. *Ph.D thesis, Department of Geography, University of Leicester, Leicester, UK.*